CHAOS IN AXIALLY SYMMETRIC NUCLEAR POTENTIAL WITH DIFFUSE SURFACE AND SPIN–ORBIT COUPLING

R. MURAT AND P. ROZMEJ

Department of Theoretical Physics, Maria Curie-Skłodowska University,
Pl. M. Curie-Skłodowskiej 1, 20-031 Lublin, Poland
<murat@tytan.umcs.lublin.pl>, <rozmej@tytan.umcs.lublin.pl>

(Received March 21. 1995; revised version received August 10, 1995)

The results for the classical single-particle motion in the Woods–Saxon potential with octupole deformation including the spin-orbit interaction are reported. The dependence of the nucleonic dynamics on the potential diffuseness and on the spin-orbit coupling is studied. The model is examined by means of qualitative (Poincaré sections) as well as quantitative (Lyapunov exponents, power spectrum) methods. The transition from order to chaos is observed when the spin-orbit coupling increases. The role of the diffuseness of the potential in suppressing chaos is also shown.

PACS numbers: 03.65. Sq, 21.60. Cs, 47.52. +j

1. Introduction

In the last few years the growing interest of application of ideas of chaos to the nuclear physics is observed. Since it has become apparent that the character of collective nuclear dynamics could be related to a nature of single-particle nucleon motion the latter has been studied in various nuclear mean field potentials [1–10]. It has been shown [1, 2] in a simple model that there is a correspondence between elastic or dissipative behaviour of nucleus as a whole and integrability or non-integrability of equations of the nucleonic single-particle motion. It indicates that for understanding collective processes it is essential to find under what conditions the motion becomes chaotic. The transition from order to chaos in single-particle motion in a mean field potential may be induced by changes of nuclear shapes [1–10] as well as by increasing the spin-orbit interaction [5–8, 10]. Most of investigations are at the classical level but some papers contain quantal studies [3, 5, 11–13].

The purpose of the present paper is to present the influence of:

- the diffuseness of the mean field potential,
- the spin-orbit coupling

on the motion of a nucleon inside nucleus. All calculations presented below are classical. The considered mean field potential is the deformed Woods-Saxon potential. In order to achieve our goals and illustrate obtained results, we concentrate our discussion on a particular family of nuclear shapes.

2. Model

2.1. Shape parametrization

In general, axially symmetric nuclear shapes may be described by means of Legendre polynomials $P_n(\cos\vartheta)$

$$R(\vartheta) = \frac{R_0}{\Lambda}[1 + \alpha_1 P_1(\cos\vartheta) + \sum_{n>1} \alpha_n P_n(\cos\vartheta)], \tag{1}$$

where Λ denotes the normalizing factor ensuring the volume conservation. The term $\alpha_1 P_1(\cos\vartheta)$, necessary only for nonzero odd n deformations, restores the centre of mass to the origin of the coordinate system. Parameter specifying the degree of deformation, α_n, depends on n in the following way $\alpha_n = \sqrt{\frac{2n+1}{5}}\,\alpha$ in order to keep the same r.m.s. deviation of the deformed surface from a sphere for all multipolarities (for small α). Such a parametrization of shape has been widely used in nuclear physics for decades. It appeared to supply a good description of a big variety of nuclear features and processes from nuclei in their ground states to fast rotating and fissioning nuclei (see *e.g.* [14–16]).

In the case of the square well potential, the single-particle motion for shapes with different order of Legendre polynomials $n = 2, 3, 4, 5, 6$ has been studied in [1, 2]. Our model can be treated as a generalization of this 3-dimensional billiard in order to include a more realistic features of a nuclear mean field. As we relate our results to those of [1, 2] let us briefly remind some of them which are relevant for a further discussion. The character of the motion was studied there for static shapes as well as for oscillating ones. The main results, we refer to, are the following. The single-particle motion undergoes a transition from order to chaos when deformation increases. For the same energy trajectories with small projection of the angular momentum on the symmetry axis become chaotic first than those with bigger projections. For higher multipole deformations the transition occurs earlier (*i.e.* for smaller values of the deformation parameter). For example the dynamics of motion with small projections of angular momentum on the symmetry

axis for $n \geq 3$ and $\alpha_n \geq 0.1$ is already almost completely chaotic for the 3-dimensional billiard. The results of present paper refer to this type of initial conditions and deformations.

2.2. Definition of potential

The single-particle Hamiltonian has the form

$$H = T + V + V_{so}\,, \tag{2}$$

where T denotes the kinetic energy and V is deformed Woods–Saxon potential defined as follows,

$$V(\boldsymbol{r}, \vartheta) = \frac{V_0}{1 + \exp[d(\boldsymbol{r}, \vartheta)/a'(\vartheta)]}\,. \tag{3}$$

The symbol V_0 denotes the depth of the potential, $d(\boldsymbol{r}, \vartheta)$ is the distance from an arbitrary point $\boldsymbol{r}$ to the surface defined by (1)

$$d(\boldsymbol{r}, \vartheta) = |\boldsymbol{r}| - R(\vartheta)\,, \tag{4}$$

and $a'(\vartheta)$ is the diffuseness in $\boldsymbol{r}$ direction, calculated to keep the skin of the potential in direction perpendicular to the surface approximately constant (equal a). In other words $a' = a/\cos(\boldsymbol{a}, \boldsymbol{a})$ as it is shown in Fig. 1. The ϑ is a polar angle in a coordinate space.

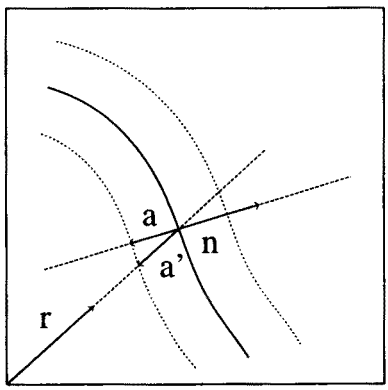

Fig. 1. Figure explaining the modification of the diffuseness of deformed potential (3) in order to keep the nuclear skin approximately constant. The diffuseness a' in the direction of position vector $\boldsymbol{r}$ is calculated to have the projection on direction perpendicular to the surface, $\boldsymbol{n}$, equal a.

And finally, V_{so} in (2) denotes the spin-orbit interaction taken in the conventional form,

$$V_{so} = \kappa(\nabla V \times \boldsymbol{p}) \cdot \boldsymbol{s}\,, \tag{5}$$

where κ is the strength of the spin-orbit coupling. The 'classical spin' $\boldsymbol{s}$ is assumed to be a vector of constant length ($^1/_2\,\hbar$) with direction defined by polar angles ϕ and θ. Then the classical Hamiltonian has the same form as the quantum one (2) and can be derived from the former applying the time-dependent variational principle [6, 17, 18].

To make our discussion more general, we take into account only particles from Fermi surface. Because of the dependence of Fermi level on the diffusion of the potential the relative units are used. Positions are expressed in units of a radius R_F corresponding to Fermi energy and momenta — in units of Fermi momentum p_F. In these units the fundamental features of the model do not depend on the particular choice of parameters of the potential (*e.g.*depth of potential or radius parameter). So finally the classical Hamiltonian (2) can be expressed by means of the dimensionless generalized cartesian coordinates (x, y, z) and the spin angle (ϕ) and the related momenta (p_x, p_y, p_z) with the spin momentum defined by $p_\phi = \frac{1}{2}\cos\theta$. The coordinates and momenta span 8-dimensional phase space. However due to the energy conservation and axial symmetry of the problem the number of degrees of freedom is reduced to six. The Hamiltonian (2) is in general non-integrable. It becomes integrable only for two particular cases: spherical and spheroidal shapes with sharp-edged potential (*i.e.* diffuseness going to zero). The equations of motion are simply the Hamiltonian equations. In our case they take the following form

$$\dot{x}_i = p_i + \kappa\,(\boldsymbol{s} \times \nabla V)_i\,, \tag{6}$$

$$\dot{p}_i = -\nabla_i V - \kappa\epsilon_{klj}\nabla_i(\nabla_k V)p_l s_j\,, \tag{7}$$

$$\dot{\phi} = -\kappa\left[((\nabla V \times \boldsymbol{p})_x \cos\phi + (\nabla V \times \boldsymbol{p})_y \sin\phi)\cot\theta - (\nabla V \times \boldsymbol{p})_z\right]\,, \tag{8}$$

$$\dot{\theta} = -\kappa\left[(\nabla V \times \boldsymbol{p})_x \sin\phi - (\nabla V \times \boldsymbol{p})_y \cos\phi\right]\,. \tag{9}$$

We solve them numerically using an adaptive stepsize Runge-Kutta method.

3. Results

In the present paper we concentrate our presentation on a particular case of the potential, such that the motion of the spinless particle in a 3-dimensional billiard is almost fully chaotic. Then varying the diffuseness parameter (a) and the spin-orbit coupling constant (κ) we can examine changes of the character of the dynamics introduced by the generalization of the model. In this task we use again relative units, a_0 and κ_0, which

correspond to the values adjusted within Woods–Saxon potential to reproduce known nuclear single-particle levels. We chose the octupole deformed shape with $\alpha = 0.1$. For other shapes (higher multipole deformations, or in general a combination of several multipole deformations) the results are qualitatively very similar when overall deformation is of the same order of magnitude.

3.1. Poincaré sections

In order to show the dependence of the motion of a particle on the diffuseness only, the spin-orbit coupling is taken to be equal zero ($\kappa = 0$). This simplification restricts the dimension of the phase space to 4, because there is no motion in the spin subspace and the motion in ordinary subspace becomes identical with the motion of a spinless particle. Let us start with practical and often used qualitative test on chaos — the Poincaré sections which are generated by recording the particle's radial distance ρ from the symmetry axis and the radial momentum p_ρ each time the particle crosses the equatorial plane $z = 0$, changing the sign of z-coordinate in the same way (*e.g.* from $z > 0$ to $z < 0$). Each panel presented in Fig. 2 corresponds to 10 trajectories starting from the points located at distances from the centre of the potential equal to $\rho_i = \frac{(i-1)}{10}\,\rho_{\mathbf{max}}$, where $i = 1, 2, \ldots, 10$ and $\rho_{\mathbf{max}}$ denotes equatorial radius, with the momentum parallel to the Oz axis, *i.e.* projection of the angular momentum on the symmetry axis $l_z = 0$. For every set of the control parameters for each trajectory over 2000 events has been noted which gives 20000 points displayed on each panel of Figs 2 and 4.

Fig. 2a shows the Poincaré sections for the diffuseness $a = 0.1$ in units of normal nuclear diffuseness a_0. The points of section fill more or less uniformly almost all approachable phase space except one region which remains empty. The random swarm of the points indicates that the motion is chaotic for most of initial conditions. Trajectories corresponding to this type of section are not restricted to the invariant tori and can penetrate all approachable phase space. The empty region is probably regular. One can observe how it evolves on next panels of Fig. 2. Almost the same situation occurs for $a = a_0$ (Fig. 2b) but there appear two more regions which are not visited by investigated trajectories at all and one closed curve corresponding to the trajectory of a particle started from the centre of the shape. This two types of regions are well seen on next panel (Fig. 2c), which refers to $a = 1.5a_0$. The regular motion is observed for few more trajectories (corresponding to the initial positions close to the symmetry axis as well as the most distant ones) which points of section compose curves. This means that some invariant tori are rebuilt due to the increase of the diffusion of the potential. The motion is now a mixture of order and chaos. The structure of phase space becomes more complex. It consists of both

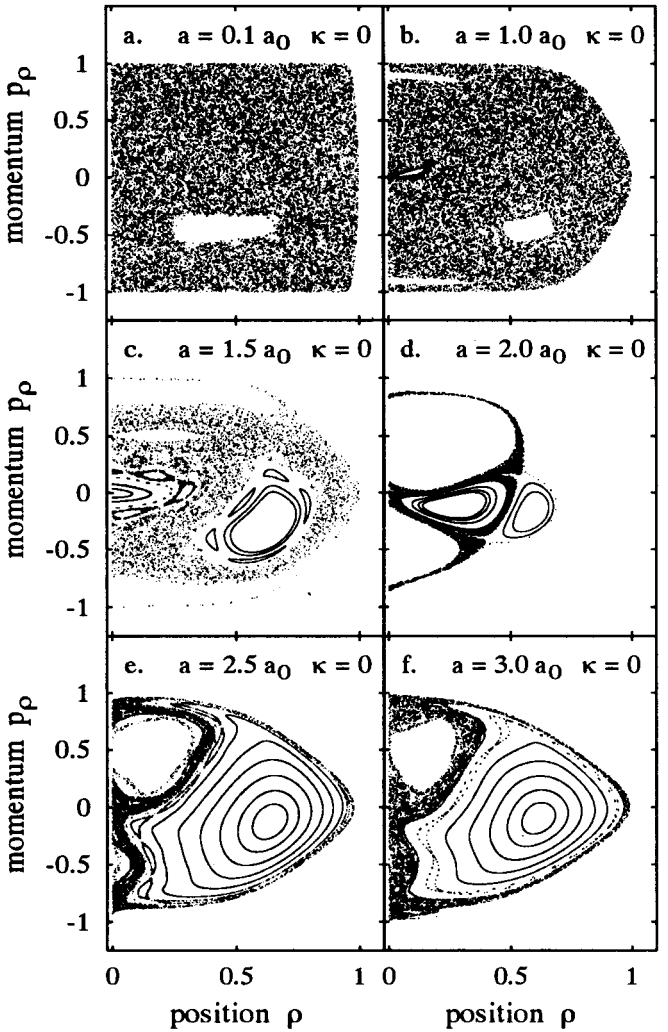

Fig. 2. Poincaré sections for 10 planar trajectories with zero projection of the orbital angular momentum on the symmetry axis ($l_z = 0$). The spin-orbit interaction strength κ=0 and the diffuseness : **a)** $a = 0.1a_0$, **b)** $a = 1a_0$, **c)** $a = 1.5a_0$, **d)** $a = 2a_0$, **e)** $a = 2.5a_0$, **f)** $a = 3a_0$.

types of regions, chaotic and regular, which are very close each other. Next figure (Fig. 2d) presents the Poincaré sections corresponding to the diffuseness $a = 2a_0$. In this case all examined trajectories are regular or almost regular. And finally we show the sections for $a = 2.5a_0$ and $a = 3a_0$, Fig. 2e and 2f, respectively. The trajectories with small initial positions be-

come more chaotic again (dots corresponding to traces of the most external curves) while trajectories started far from the symmetry axis are regular. The role of diffuseness in suppressing chaos can be explained by a fact, that for smaller values of a the change of nonlinear force during the 'reflection' from the surface is much more violent than in the case of bigger diffuseness. The exemplary planar trajectories represented in the meridian plane in (x, z) coordinates for $a = 0.1a_0$ and $a = 3a_0$ are displayed in Fig. 3. The starting point is $\rho = {}^1/_2\,\rho_{\max}$ in both cases. It should be emphasized that these are very short fragments of trajectories in question presented to show the differences between them. For longer time of evolution they both cover thickly the explored region. For smaller value of the diffuseness parameter trajectory can penetrate wider part of the phase space. The trajectory is similar to that one resulting from a sharp-walled billiard: it consists of the points of reflection and straight lines between them. For larger a the trajectory creates a regular pattern. It is smoother, the change of the force is 'softer', like in a deformed harmonic oscillator potential.

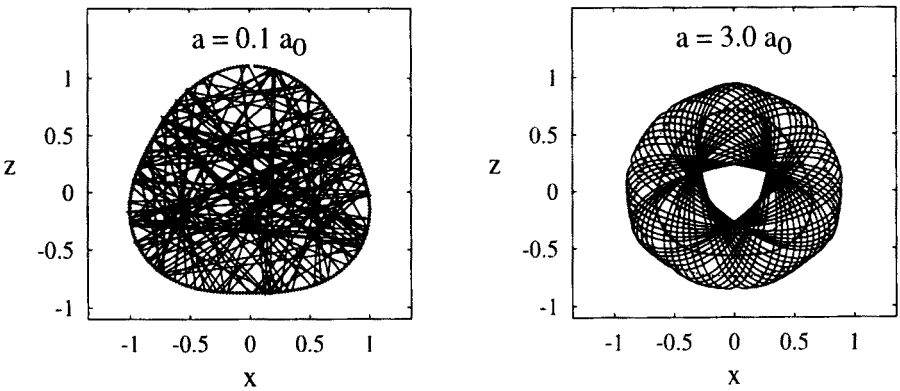

Fig. 3. Exemplary trajectories for $a = 0.1a_0$ (left panel) and $a = 3a_0$ (right panel).

In order to show the dependence of the nucleon motion on the spin-orbit coupling, we use the previous results and examine what happens with the motion in the case with partially regained regularity due to the increase of the diffuseness of potential, namely $a = 3a_0$, when the parameter κ differs from zero. Just as in Fig. 2 the Poincaré sections have been obtained for 10 trajectories with the same initial conditions. However, when the spin-orbit interaction is switched on, the dimension of the phase space increases to 6 (8 minus 2 constants of motion in involution). Therefore the dimension of Poincaré sections increases to 4, and what we show are two 2-dimensional projections of this sections on the ordinary (Fig. 4a, 4c, 4e) and

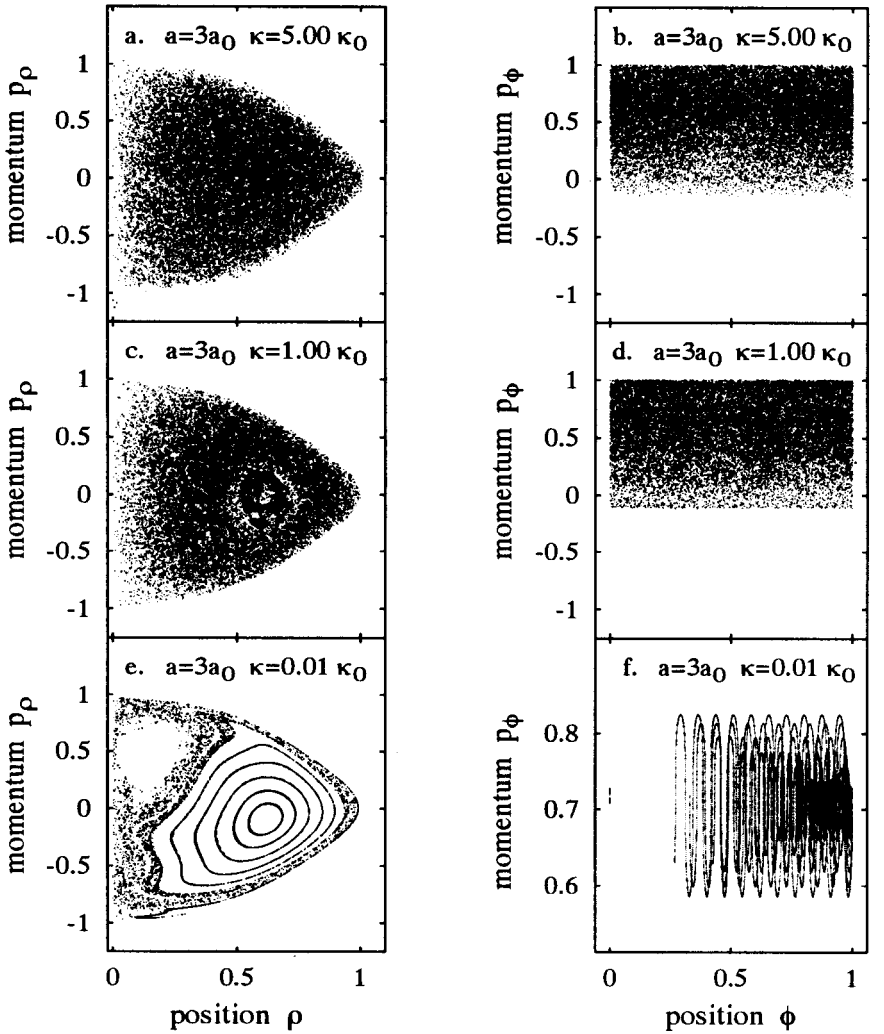

Fig. 4. Poincaré sections for 10 trajectories with the same projection of the total angular momentum on the symmetry axis. Left part (a, c, e) shows the projections of the sections onto the ordinary subspace and right-hand one (b, d, f) — onto the spin subspace. The diffuseness $a = 3a_0$ and the strength of the spin-orbit coupling: **a,b** $\kappa = 5\kappa_0$, **c,d** $\kappa = \kappa_0$, **e,f** $\kappa = 0.01\kappa_0$.

spin (Fig. 4b, 4d, 4f) subspaces, in the same way as in [6–8]. The Poincaré sections presented in Fig. 4e refers to $\kappa = 0.01\ \kappa_0$, where κ_0 denotes normal value of the strength of the spin-orbit coupling. Comparing Fig. 2f with Fig. 4e one sees that switching the spin-orbit interaction on with very

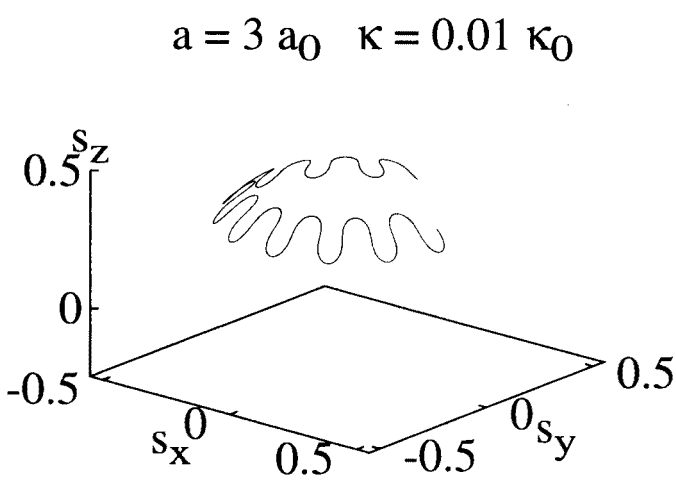

Fig. 5. Projection of the Poincaré section on the spin sphere. The single trajectory, which other projection of the Poincaré section form the most inner curve in Fig. 4e, is shown.

small intensity (1% of average nuclear value), leaves most of regular orbits untouched. The degree of a nonlinearity introduced by this week coupling is, in general, not sufficient to destroy these tori of regular motion. The closer look reveals, however, that even such week coupling broadens areas of chaotic motion. The complementary projection of the section on spin subspace, Fig. 4f, indicates a regular motion for this set of control parameters and initial conditions. However, the concluding from the Poincaré section for higher phase space dimension is not as obvious as for two-dimensional one. The additional calculations of the Lyapunov exponents and the power spectra show, that most of trajectories shown in Figs. 4e and 4f represent indeed a regular motion. It could be also seen in Fig. 5, where the points of section originating from the same trajectory as points forming the most inner curve in Fig. 4e, presented in the spin space on the 'spin sphere' form a very regular pattern. When the spin-orbit coupling reaches its normal nuclear strength the sections show, Fig. 4c and 4d, that the tori of regular motion are already destroyed. The sections in spin variables suggest the complete chaoticity of the motion and these in ordinary variables show only the traces of some of the most stable tori as the regions with higher density of points. For unnaturally strong spin-orbit coupling, the loss of regularity is complete in both subspaces, Fig. 4a and 4b. Even the most stable tori are destroyed. Results shown in Fig. 4 are the same as conclusion of the papers [5–8] that spin-orbit coupling is a source of chaos in classical dynamics of a nucleon in the deformed potential.

3.2. Lyapunov exponents

The above results can be confirmed by means of quantitative methods of detecting chaos presented below. First one is the Lyapunov exponents method which is a useful tool for an analysis of stability properties of trajectories. The Lyapunov exponents measure the average ratio of an exponential divergence (or convergence) of trajectories with nearly identical initial conditions in the limit when time, over which the averaging is performed, tends to infinity and the difference between initial conditions tends to zero [19]. Generally, in N-dimensional phase space there exists a spectrum of N Lyapunov exponents. For a Hamiltonian system, as a consequence of the phase space volume conservation, they must appear in pairs, $\lambda_i = -\lambda_{N+1-i}$ ($\lambda_1 > \lambda_2 > \ldots > \lambda_N$). The motion is chaotic (for a given trajectory) if at least one exponent is positive. Therefore, to detect chaos it is enough to calculate the maximal Lyapunov exponent, which is much easier and less time consuming task than calculating the whole spectrum.

We determine the largest Lyapunov exponent by the method of Benettin *et al.* [20], which consists of evolving two trajectories initially separated by d_0 for the time interval Δt, after which the magnitude of the distance between them (Δt) is rescaled back to d_0. The procedure is repeated k times. The maximal Lyapunov exponent is expressed in the following form

$$\lambda_{\max}(t) = \lim_{d_0 \to 0} \lim_{k \to \infty} \frac{1}{k\Delta t} \sum_{i=1}^{k} \ln \frac{d_i(\Delta t)}{d_0}. \tag{10}$$

The metric used to calculate d is the cartesian one with a small modification, namely $\Delta\phi$ is taken modulo 2π and together with p_ϕ scaled to the same range as other variables. In our calculations the renormalization time interval $\Delta t = {}^1\!/_2\tau_0$, where $\tau_0 = \frac{R_F}{v_F}$ is the unit of time.

Left panel in Fig. 6 shows the maximal Lyapunov exponents for $\kappa = 0$ and three values of the diffuseness parameter $a = 0.1a_0, 1a_0$ and $3a_0$ and right-hand one refers to $a = 3a_0$ and three values of the spin-orbit coupling strength $\kappa = 0.01\kappa_0, 1\kappa_0$ and $5\kappa_0$. The exponents are determined by 100 random trajectories in each case (*nt* in Fig. 6 denotes the serial number of trajectory and have no special meaning). They are chosen to belong to the same class as previously tested ones (trajectories of particles from Fermi surface with the zero projection of the orbital angular momentum on the symmetry axis). When the spin-orbit interaction is not taken into account ($\kappa = 0$) the largest values of the maximal exponent are obtained for the smallest diffuseness. All trajectories for $a = 0.1a_0$ are more or less chaotic — they lead to finite, positive values of $\lambda_{\max}$. Like in 3-dimensional billiard [2] with the same initial conditions, Lyapunov exponents are substantially

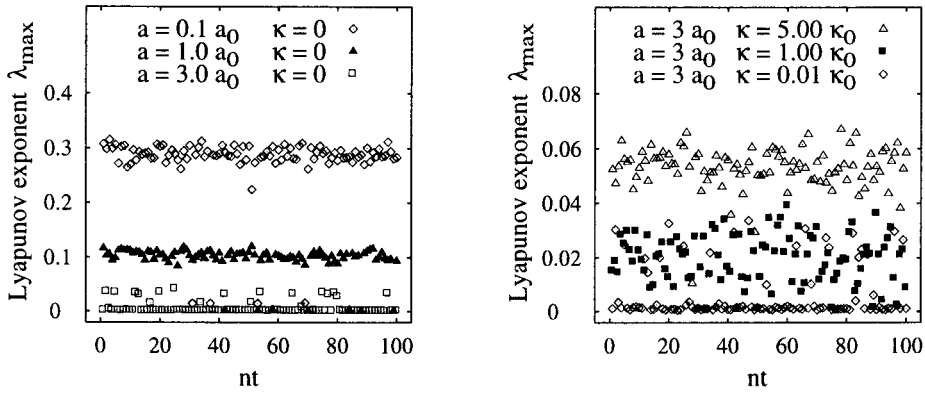

Fig. 6. The maximal Lyapunov exponents determined by 100 random trajectories for each set of control parameters. **Left:** $a = 0.1a_0, 1a_0, 3a_0$ and $\kappa = 0$. **Right:** $a = 3a_0$ and $\kappa = 0.01\kappa_0, 1\kappa_0, 5\kappa_0$.

big. However, there also exist a few trajectories with small but finite $\lambda_{\max}$ (greater then 10^{-3}). For $a = a_0$, the maximal Lyapunov exponents also indicate chaotic behaviour although the values of $\lambda_{\max}$ are smaller than in the previous case, except a few of them which are nearly zero, suggesting that some trajectories may be close to the rebuilt tori in phase space. For the biggest considered value of the diffuseness parameter ($a = 3a_0$) most initial conditions lead to very small $\lambda_{\max}$ (less then 10^{-3}). For such a case it is very difficult to determine numerically the 'true' value of the exponent, defined as limit over infinite time. The logarithmic plots suggest, however, that this limit is rather zero, than a finite value. But even in this case there are still trajectories for which finite Lyapunov exponents are obtained. The above results confirm that motion becomes more regular with increase of thickness of the potential skin for the considered class of initial conditions. The regained regularity is destroyed by switching the spin-orbit interaction on and increasing its strength. The right-hand panel of Fig. 6 illustrates that when we start from a partially regular motion in a deformed potential, the growing strength of the spin-orbit coupling increase chaoticity of the motion. For $\kappa = 0.01\kappa_0$ there are some nonzero exponents, but already more, than for $\kappa = 0$ and the same a (the most regular case in Fig. 6, left). For $\kappa = \kappa_0$, chaos is already developed, in spite of the large diffuseness, however some trajectories are still regular. And finally for the strong coupling, $\kappa = 5\kappa_0$, the Lyapunov exponents are big again.

In all papers, treating up to now nuclear models in classical terms, at most one positive Lyapunov exponent (the maximal one) has been found [1,2,5–9]. In our model, as it is shown in Fig. 7, there exist trajectories for

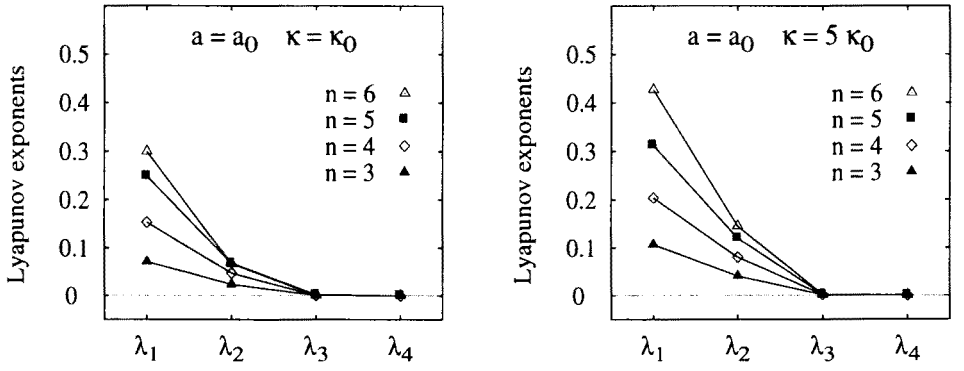

Fig. 7. The spectra of Lyapunov exponents for different deformation types ($\alpha = 0.1$ and $n = 3, 4, 5, 6$) and spin-orbit couplings (**left:** $\kappa = \kappa_0$; **right:** $\kappa = 5\kappa_0$). All results correspond to the same type of orbit (the same j_z).

which two positive exponents occur. In this figure we present only positive Lyapunov exponents (negative exponents are symmetrical to the positive ones due to the phase space volume conservation) calculated for the trajectories belonging to the same class as previously tested ones. For all types of considered deformation ($n = 3, 4, 5, 6$) the initial conditions are chosen in the same way as for the sixth trajectory displayed in Fig. 4. All presented results correspond to the same deformation parameter $\alpha = 0.1$ and normal nuclear diffuseness ($a = a_0$). The left part shows Lyapunov exponents for the normal nuclear value of the spin-orbit coupling ($\kappa = \kappa_0$), the right-hand one those obtained for a strong coupling ($\kappa = 5\kappa_0$). The spectrum of Lyapunov exponents has been determined by evolving in time a small phase space volume and investigating rates of its expansion and contraction in the orthogonal directions [19]. The phase-space volume conservation (Liouville's theorem) served us also as a convenient test of a quality of the numerical integration. The sum of all Lyapunov exponents was always zero, with accuracy better than 10^{-5}. From Fig. 7 it is clear, that in our model, the trajectories with two positive exponents exist. The case with increased spin-orbit coupling confirm this conclusion doubtless. The trend, observed in a model without spin [1, 2], that the degree of chaos increases with the multipolarity of a deformation (n) is confirmed. In papers [6–8] we have shown, that for deformations preserving the integrability of a potential, the spin-orbit forces are a source of a chaotization of motion. In present model, there is an additional source – the type of deformation making the potential non-integrable (even for $\kappa = 0$).

3.3. The power spectrum

Another powerful, yet rather seldom used, method of investigation the character of a dynamics is the Fourier analysis. After recording the phase space coordinates in small equidistant time steps one is able to perform a frequency analysis of the resulting time series. Let us show an example of such an analysis for the same values of control parameters (diffuseness and spin-orbit coupling strength) for which the Poincaré sections and the Lyapunov exponents have been already presented. Let us consider a typical trajectory, with initial conditions $\rho = {}^1\!/_2\ \rho_{\mathbf{max}}$ and only nonzero momentum p_z (belonging to the same class of initial conditions as trajectories used to calculate the Poincaré sections and the spectrum of Lyapunov exponents).

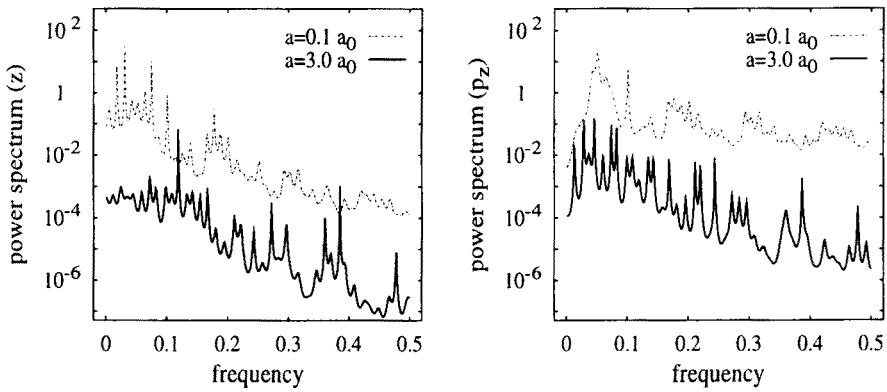

Fig. 8. The power spectra of $z(t)$ and $p_z(t)$ — time series for $a = 0.1a_0$ (dashed line) and $a = 3a_0$ (solid line).

In Fig. 8 we show power spectra of time series of z-coordinate and p_z-momentum for the diffuseness $a = 0.1a_0$ and $a = 3a_0$, respectively. The power spectra have been calculated using the maximum entropy method, as described in [21]. For a small diffuseness the power of both coordinate and momentum time series is distributed more or less uniformly in the whole region of frequencies (which is limited by the length of recorded data). This behaviour shows that there is no regular motion. In contrast, the power of the corresponding signals obtained for the diffuse potential with the thick skin is composed of a sequence of well distinguished peaks, corresponding to characteristic frequencies. This is typical for regular motion on tori in a multidimensional space. In Fig. 9 we display the power spectra for motion with the spin-orbit coupling switched on. In this case, the dimension of the phase space is higher and besides time series of the spatial variables one can investigate time series of variables in the spin subspace. The former is shown

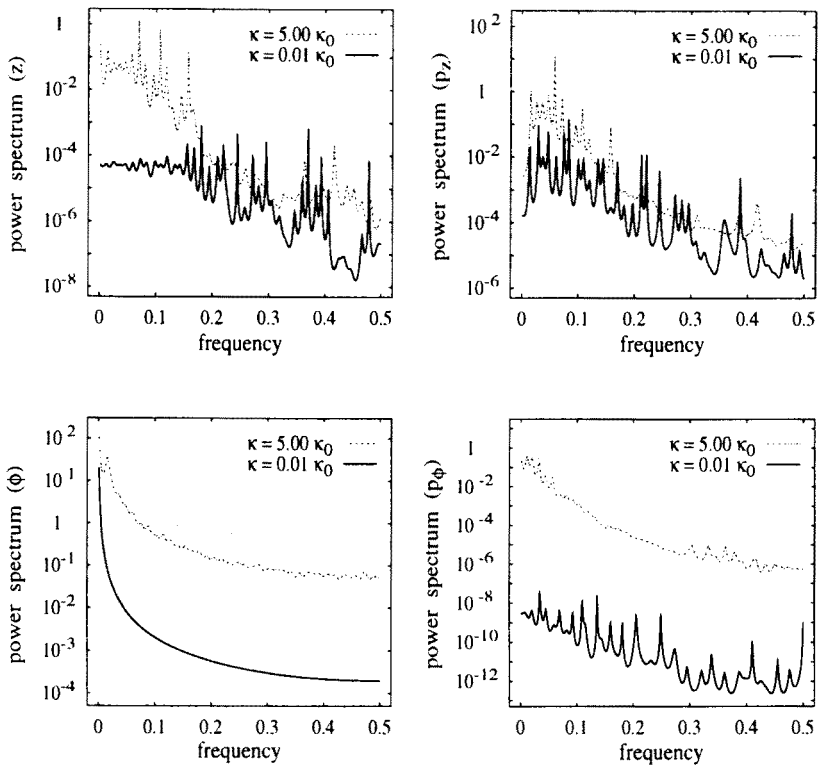

Fig. 9. The power spectra of $z(t)$, $p_z(t)$, $\phi(t)$, $p_\phi(t)$ — time series for $a = 3a_0$ and $\kappa = 0.01\kappa_0$ (solid line) and $\kappa = 5\kappa_0$ (dashed line).

in the upper part and the latter in the lower part of Fig. 9, for $\kappa = 0.01\kappa_0$ and $\kappa = 5\kappa_0$ and $a = 3a_0$. Again, like in Fig. 8, we have two different types of spectra, representing a regular motion for the weak coupling and chaotic one for the strong coupling. The difference is particularly evident in the power spectra connected to the signals from the spin subspace.

4. Conclusions

In the present paper we discuss some features of a single-particle motion in a deformed, axially symmetric potential. The realistic nuclear potential have been examined, and the dependence of the single-particle nucleonic motion on a thickness of a nuclear skin and on a strength of the spin-orbit coupling has been presented. The following conclusions can be drawn:

For well deformed shapes, when the single-particle motion is chaotic in 3-dimensional billiard case, an increase of the skin thickness within a wide

range of values leads towards restoration of regularity. This effect is due to less rapid changes of forces acting at the surface in case of a diffuse potential (both forces from the potential and from the spin-orbit interaction). One should remember, however, that for a particular spherical and spheroidal shapes, assuring integrable motion, the diffuseness, introducing nonlinear terms to an integrable Hamiltonian acts in the opposite way [3, 4] (*i.e.* as a source of a week chaos in the system).

The spin-orbit interaction, as a strongly nonlinear force, acts always as a source of chaos in a single-particle dynamics. There was shown in [6–8] that in an integrable deformed potential, the spin-orbit interaction only is enough, for reasonable coupling strength, to make the dynamics chaotic. Present investigations show that, for more realistic potentials, taking into account a richer family of nuclear shapes, a classical motion of a particle with spin could be chaotic for quite moderate deformations. The influence of underlying chaotic dynamics on nuclear properties should be the strongest, however, for shapes far from spherical symmetry.

For the reason of transparency and compactness, we illustrated our investigations mostly with a particular choice of the octupole deformation. Qualitatively, we observe very similar influence of the diffuseness and the spin-orbit coupling strength on the character of a dynamics also for more complicated shapes (*i.e.* shapes described by $\alpha_4, \alpha_5, \alpha_6$ and in general shapes determined by several multipoles). In all cases, the spin-orbit interaction enhances chaos observed already in simpler potentials [1, 2, 9].

Our study of the full spectrum of Lyapunov exponents shows, that when a non-integrable deformation and spin-orbit coupling act together, the degree of chaos increases. In this case a chaotic single-particle motion characterized by two positive Lyapunov exponents is possible.

The authors are grateful to R. Arvieu, J. Blocki, W. Nörenberg and A. Sobiczewski for helpful discussions and valuable comments.

REFERENCES

[1] J. Błocki, J.J. Shi, W.J. Świątecki, *Nucl. Phys.* **A554**, 387 (1993).
[2] J. Błocki, F. Brut, T. Srokowski, W.J. Świątecki, *Nucl. Phys.* **A545**, 511c (1992).
[3] R. Arvieu, F. Brut, J. Carbonell, J. Touchard *Phys. Rev.* **A35**, 2389 (1987).
[4] J. Carbonell, F. Brut, R. Arvieu, J. Touchard *J. Phys.* **45**, C6-371 (1984).
[5] B. Milek, J. Reif, *Z. Phys.* **A339**, 231 (1991).
[6] P. Rozmej, R. Arvieu, *Nucl. Phys.* **A545**, 497c (1992).
[7] R. Arvieu, P. Rozmej, M. Płoszajczak, in *New Trends in Theoretical and Experimental Physics*, Predeal Summer School 1991, World Scientific, Singapore 1992, p. 232.

[8] P. Rozmej, R. Arvieu, *Acta Phys. Pol.* **B25**, 759 (1994).
[9] W.D. Heiss, R.G. Nazmitdinov, S. Radu, *Phys. Rev. Lett.* **72**, 2351 (1994).
[10] H. Frisk, T. Guhr, *Ann. Phys.* (NY) **221**, 229 (1993).
[11] B. Milek, W. Nörenberg, P. Rozmej, *Z. Phys.* **A334**, 233 (1989).
[12] R. Arvieu, P. Rozmej, *Phys. Rev.* **A50**, 4376 (1994).
[13] R. Arvieu, P. Rozmej, *Phys. Rev.* **A51** (in print, January 1995).
[14] M.J.A. de Voigt, J. Dudek, Z. Szymański, *Rev. Mod. Phys.* **55**, 949 (1983).
[15] A. Sobiczewski, Z. Patyk, S. Ćwiok, P. Rozmej, *Nucl. Phys.* **A485**, 16 (1988).
[16] S. Ćwiok, P. Rozmej, A. Sobiczewski, Z. Patyk, *Nucl. Phys.* **A491**, 228 (1989).
[17] H. Kuratsuji, T. Suzuki, *J. Math. Phys.* **21**, 472 (1990).
[18] H. Feldmeier, *Nucl. Phys.* **A515**, 147 (1990).
[19] A.J. Lichtenberg, M.A. Liberman, *Regular and Stochastic Motion*, Springer-Verlag, 1983.
[20] G. Benettin, L. Galgani, J.M. Strelcyn, *Phys. Rev.* **A14**, 2338 (1976).
[21] W.H Press, B.P. Flannery, S.A. Teukolsky, W.T. Vettering, *Numerical Recipes*, Cambridge University Press, Cambridge 1986.